Mathematical modeling of long waves in an irregular shaped harbor using boundary element method

Cite as: AIP Conference Proceedings **2435**, 020016 (2022); https://doi.org/10.1063/5.0083545
Published Online: 18 March 2022

Prashant Kumar, Divya Sardana and Rajni

Mathematical Modeling of Long Waves in an Irregular Shaped Harbor using Boundary Element Method

Prashant Kumar[1, a)], Divya Sardana[1, b)], Rajni[2, c)]

[1]*Department of Applied Sciences, National Institute of Technology Delhi, Delhi-110040, India*
[2]*Jindal Global Business School, O P Jindal University, Sonipat, Haryana, India*

[a)]Corresponding author: *prashantkumar@nitdelhi.ac.in*
[b)] *divyasardana@nitdelhi.ac.in*
[c)] *rajni@jgu.edu.in*

Abstract. A mathematical model has been developed to study the theoretical analysis of long waves in a complex geometrical port. The domain of interest is categorized into sub regions and wave functions are evaluated individually in both the regions. Boundary element method is employed to solve the integral equations by utilizing the kinematic and dynamic boundary conditions. The integral equations are further converted into a system of linear equations. The domain is discretized non-uniformly to obtain the optimum accuracy. The solution is obtained by equating the matching conditions at the entrance of the harbor, by using the continuity conditions of the irrotational flow of an incompressible fluid. The theoretical results of the problem obtained from the BEM for the rectangular domain have been verified with studies done by Lee (1971). Based on the validation, the present numerical model is implemented on real domain as Paradip port, Odisha, India for practical applications.

INTRODUCTION

Ocean waves propagating from open sea into the port cause a significant damage to the moored ships, coastal structures and the boundaries. The extreme incident wave amplitude originating from the strong typhoons induce undesirable movement of ships and create disturbances in loading/unloading of moored ships. One of the majorly affected ports is the Paradip port located on the coast of Bay of Bengal in Odisha, India. It experiences the direct incoming of long waves which are strong enough to hinder the operations at the harbor, especially during weather conditions.

Many attempts have been made to study the resonance in ports of different geometry. The impacts of these oscillations have been studied by various numerical models [1-4]. These models are based on Finite Element Method (FEM), Boundary Element Method (BEM), Mild Slope Equation (MSE) or modified MSE [5,6], Lagrange equations etc. BEM and Helmholtz equation is utilized to analyze an arbitrary shaped harbor with constant depth problems [7-11] whereas time dependent MSE is also utilized [12, 13]. Numerical studies based on harbor resonance for multidirectional random waves has also been investigated [14,15].

Recently, models have been constructed to study realistic harbors, for instance, Pohang New Harbor in South Korea [16-18], Port of Ferrol in Spain [19], Hua-lien harbor in Taiwan [8], Marina di Carrara harbor in Italy [2], Paradip port in India [20, 21] analyzed the wave induced oscillations of water wave in complex geometrical port using Hybrid FEM. Higher order FEM is used to analyze the propagation of waves excited by internal elements [22].

In this article, Helmholtz equation is formulated in a bounded domain corresponding to prescribed boundary conditions. Analytical approximations have been carried out to compare the theoretical results with the current numerical scheme. To enhance the numerical accuracy, the periphery of Paradip port is discretized into irregular elements and refined near the corner points. Further, present model is also implemented on Paradip port.

Proceedings of the Third International Conference on Frontiers in Industrial and Applied Mathematics 2020
AIP Conf. Proc. 2435, 020016-1–020016-9; https://doi.org/10.1063/5.0083545
Published by AIP Publishing. 978-0-7354-4177-4/$30.00

MATHEMATICAL FORMULATIONS

Considering the irrotational flow and incompressible fluid, the mathematical formulations are initiated by suggesting a solution for the Laplace equation as:

$$\varphi(x,y,z,t) = \frac{-F(x,y)Z(z)e^{-i\sigma t}}{i\sigma}, \tag{1}$$

where σ is the angular frequency, T represents wave period, $F(x,y)$ is the wave function, i is an imaginary number. By imposing the prescribed boundary conditions i.e. $\frac{\partial \varphi}{\partial n} = 0$ and using Eq. (1), the Helmholtz equation is derived as:

$$\frac{\partial^2 F}{\partial x^2} + \frac{\partial^2 F}{\partial y^2} + k^2 F = 0, \tag{2}$$

$$\frac{\partial^2 Z}{\partial z^2} = k^2 Z, \tag{3}$$

where k is denoted as the wave number i.e. $k = \frac{2\pi}{L}$ & L is the wave length. Using the boundary conditions at the bottom; the solution of Eq. (3) is as follows:

$$Z(z) = B_o \cosh k(h+z), \tag{4}$$

where B_0 is an unknown constant and making use of the dynamic free surface conditions, we obtain:

$$B_O = -\frac{B_i g}{\cosh(kh)}, \tag{5}$$

where B_i is the incident wave amplitude, g is a gravitational constant. Using Eq. (1), (4) and (5), the velocity potential function is written as:

$$\varphi(x,y,z,t) = \frac{-1}{i\sigma}\frac{B_i g \cosh k(h+z)}{\cosh kh} F(x,y)e^{-i\sigma t}. \tag{6}$$

Also, using the linearized form of the kinematic condition (z=0) for the small amplitude; a "dispersion relation" for water waves is given as follows:

$$\sigma^2 = gk \tanh(kh). \tag{7}$$

To determine the velocity potential function given in Eq. (6), wave field $F(x,y)$ satisfies the Helmholtz equation based on the following prescribed conditions:

(i) Boundary conditions along all the fixed boundaries $dF / \partial n = 0$.

(ii) As $\sqrt{x^2 + y^2} \to \infty$, i.e. the radiated wave emanating at the entrance decay at infinity.

Geometry of Model

The geometry of the study domain is categorized into two regions; Region I is an unbounded ocean region and Region II is bounded by the periphery of harbor. Wave function F_1 is estimated in Region I in terms of $\partial F_2 / \partial n$ & wave field is determined in Region II in terms of $\partial F_2 / \partial n$ at the entrance of harbor. Using the matching conditions on the entrance of the harbor; we obtain $F_1 = F_2$ & $\frac{\partial F_1}{\partial n} = -\frac{\partial F_2}{\partial n}$ where the negative sign depicts the sign convention of the normal derivative. To determine the wave function F_2 in Region II; it is sufficient to determine the normal derivative $\partial F_2 / \partial n$ at the harbor entrance. So, our main aim is to find the solution of the wave function in both the regions and then develop a procedure for equating at port's entrance.

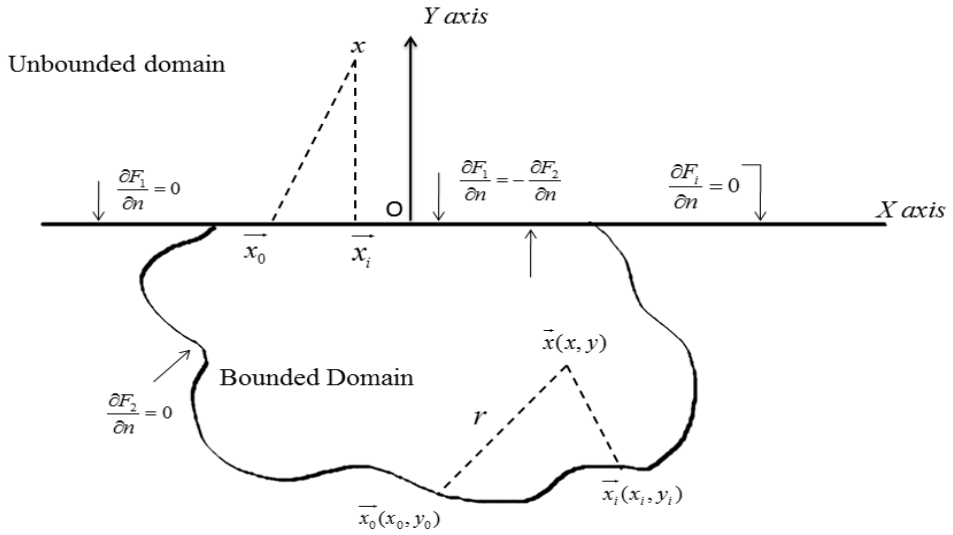

FIGURE 1. Definition sketch of an arbitrary shaped harbor.

Wave Function in Bounded Region

Consider ∂D is closed curve bounded by domain D in the *xy* plane. The wave function F_2 is determined by utilizing Green's identity theorem, and the Hankel function of 1st kind and zeroth order, $H_0^{(1)}(kr)$ which satisfies the Helmholtz equation. Due to the presence of logarithmic singularity of Hankel function, the Green's Identity is applied within the domain D_a (bounded externally by ∂D and internally by ρ_0) instead of domain D, where F and G are functions, so the integral form becomes:

$$\int_{\partial D}\left(F\frac{\partial G}{\partial n}-G\frac{\partial F}{\partial n}\right)ds+\int_{\rho_0}\left(F\frac{\partial G}{\partial n}-G\frac{\partial F}{\partial n}\right)ds=\iint_{D_a}(F\nabla^2 G-G\nabla^2 F)dxdy. \tag{8}$$

Since, the singularity lies outside the domain D_a, so take $g=H_0^{(1)}(kr)$ and we obtain:

$$\int_{\partial D}\left[F\frac{\partial}{\partial n}(H_0^{(1)}(kr))-(H_0^{(1)}(kr))\frac{\partial F}{\partial n}\right]ds+\int_{\rho_0}\left[F\frac{\partial}{\partial n}(H_0^{(1)}(kr))-(H_0^{(1)}(kr))\frac{\partial F}{\partial n}\right]ds=0 \tag{9}$$

Now on simplifying and utilizing the asymptotic behavior of Hankel function, the wave function in the bounded domain can be derived from Eq. (9) as:

$$F_2(\vec{x})=-\frac{i}{4}\int_{S'}[F_2(\vec{x_0})\frac{\partial}{\partial n}(H_0^{(1)}(kr))-H_0^{(1)}(kr)\frac{\partial}{\partial n}(F_2(\vec{x_0}))]ds(\vec{x_0}), \tag{10}$$

where $i=\sqrt{-1}$, $\vec{x_0}$ is the source point (x_0,y_0) at boundary, $\vec{x}$ is a field point (x,y) interior of the port, $F_2(\vec{x_0})$ is the wave field at the position $\vec{x_0}$, $F_2(\vec{x})$ is the wave function at position $\vec{x}$, $\frac{\partial}{\partial n}(F_2(\vec{x_0}))$ is the derivative at $\vec{x_0}$.

To find F_2 at the boundary; the above equation is made use of by approaching the field point to a $\vec{x}(x_j,y_j)$ from the interior and hence the equation holds:

$$F_2(\vec{x_i})=-\frac{i}{2}\int_{S}[F_2(\vec{x_0})\frac{\partial}{\partial n}(H_0^{(1)}(kr))-H_0^{(1)}(kr)\frac{\partial}{\partial n}(F_2(\vec{x_0}))]ds(\vec{x_0}) \tag{11}$$

This integral is approximated by partitioning the boundary into a finite number of segments and can be evaluated from Eq. (11) as:

$$F_2(\vec{x_i}) = -\frac{i}{2}\sum_{j=1}^{N}\left[F_2(\vec{x_j})\frac{\partial}{\partial n}(H_0^{(1)}(kr_{ij})) - H_0^{(1)}(kr_{ij})\frac{\partial}{\partial n}(F_2(\vec{x_j}))\right]\Delta s_j, \tag{12}$$

And hence, the corresponding matrix obtained from Eq. (12) is given by:

$$Y = a_o[S_n - SP], \tag{13}$$

$$\Rightarrow (a_o S_n - I)Y = a_o SP, \tag{14}$$

$$\Rightarrow Y = (a_o S_n - I)^{-1} a_o SP, \tag{15}$$

where $Y = F_2(\vec{x_i})$, $(S_n)_{ij} = \frac{\partial}{\partial n}(H_0^{(1)}(kr_{ij}))\Delta s_j$, $P = \frac{\partial}{\partial n}(F_2(\vec{x_j}))$, $(S)_{ij} = H_0^{(1)}(kr_{ij})\Delta s_j$, $a_0 = -\frac{i}{2}$ for $i = 1, 2, ...N$

Hence, on further simplification from Eq. (15) we obtain:

$$Y = (a_o S_n - I)^{-1} a_o SU_m.C, \tag{16}$$

$$\Rightarrow Y = MC, \tag{17}$$

where $U_m C = \sum_{j=1}^{p}\delta_{ij}c_j$, δ_{ij} is the Kroneckar delta and $M = (a_o S_n - I)^{-1} a_o SU_m$.

Thus, wave function F_2 is written as the function of normal derivatives $\frac{\partial}{\partial n}(F_2(\vec{x_j}))$ at the entrance in summation form given by:

$$F_2(\vec{x_i}) = \sum_{j=1}^{p} M_{ij}C_j, \tag{18}$$

where *p* is total segment division of entrance.

Wave Function Outside the Harbor

Using the dynamic free surface condition, the wave amplitude is represented as:

$$\eta = B_i(F_i + F_r + F_3)e^{-i\sigma t}, \tag{19}$$

where F_i is the incident wave function , F_r is the reflected wave function & F_3 is the radiated wave function. Incident wave function can be represented as $\frac{1}{2}\cos my$ for $\alpha = 90^o$ whereas the reflected wave function can be expressed as $F_r(x, y) = F_i(x, -y)$. Transforming all the boundary conditions of wave function F_1 into radiated wave function F_3, we obtain:

$$\frac{\partial^2 F_3}{\partial x^2} + \frac{\partial^2 F_3}{\partial y^2} + m^2 F_3 = 0, \tag{20}$$

along with the corresponding boundary conditions as:

(i) $\frac{\partial F_3}{\partial n} = 0,$

(ii) $\frac{\partial F_3}{\partial n} = -\frac{\partial F_2}{\partial n},$

(iii) $\lim_{x\to\infty} F_3 = 0$ & $r^2 = x^2 + y^2,$

Hence, the radiated wave function F_3 can be expressed in a similar fashion as was done for F_2 in Region II. Therefore,

$$F_3(\vec{x}) = -\frac{i}{4}\int_{S'}[F_3(\vec{x_0})\frac{\partial}{\partial n}(H_0^{(1)}(kr)) - H_0^{(1)}(kr)\frac{\partial}{\partial n}(F_3(\vec{x_0}))]ds(\vec{x_0}), \tag{21}$$

where *r* denotes the distance between two points. Also, on x-axis we have:

$$F_3(x_i, 0) = -\frac{i}{2}\int_{S'}[F_3(x_0, 0)\frac{\partial}{\partial n}(H_0^{(1)}(kr)) - H_0^{(1)}(kr)\frac{\partial}{\partial n}(F_3(x_0, 0))]ds(x_0, 0), \tag{22}$$

Using boundary conditions Eq. (22) can be represented as,

$$F_3(x_i,0) = -\frac{i}{2}\sum_{j=1}^{p} H_{ij}C_j, \tag{23}$$

where $H_{ij} = H_0^{(1)}(kr)\Delta s_j$ & $C_j = \frac{\partial}{\partial n}F_2(x_0,0)$.

On simplification, we get

$$F_1(\vec{x_i}) = 1 - \frac{i}{2}\sum_{j=1}^{p} H_{ij}C_j, \tag{24}$$

where $i = 1,2,.....p$.

Matching Conditions

From the continuity, we can derive the matching boundary condition, using Eq. (18) and (24), equating the values of wave function F_1 and F_2, we get the following equation:

$$M_p C = 1 + a_0 HC, \tag{25}$$

$$\Rightarrow C = (M_p - a_0 H)^{-1}.1, \tag{26}$$

Now, we define the "amplification factor" as:

$$R = \frac{|\eta_2(x,y,t)|}{|B_i(F_i + F_r)e^{-i\sigma t}|} = \frac{|B_i F_2(x,y)e^{-i\sigma t}|}{|B_i.1.e^{-i\sigma t}|} = |F_2(x,y)|, \tag{27}$$

where $\eta_2(x,y,t)$ denotes the wave amplitude at (x,y) interior of the port.

NUMERICAL VALIDATION AND CONVERGENCE

Considering a rectangular domain with l=12.25 in. and b=2.37 in. of depth 10.23 in., the order of convergence of current numerical model is evaluated by using the method of least squares. The periphery of the harbor is discretized into M_1=50, M_2=100 and M_3=200 regular line segments where M_1, M_2 and M_3 are discrete non-uniform finite segments. It is observed that as the number of segments is increased, the error norm is eventually decreased. The logarithmic error norm and the error norm are represented in Fig. 2 and it is found that the order of convergence is 1.77. Simultaneously, the amplification factor is also evaluated for this rectangular domain at point w (back of the wall). In Fig. 3, the present numerical scheme is compared with Lee's experiment (1971) where the ordinate denotes the amplification factor. The results have demonstrated that the current numerical scheme agrees well with the analytic approximation and Lee's experiment (1971). Thus, the current numerical model can be applied on realistic harbors as well.

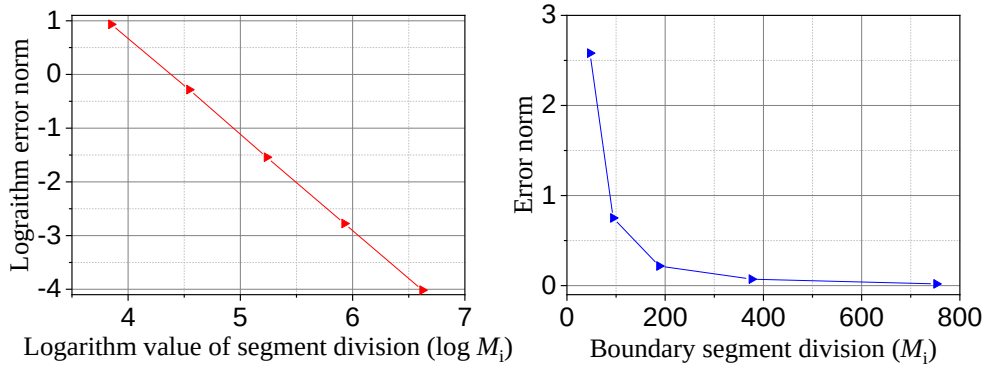

FIGURE 2. Logarithmic error norm and error norm is provided with respect to the number of segment divisions (logarithmic).

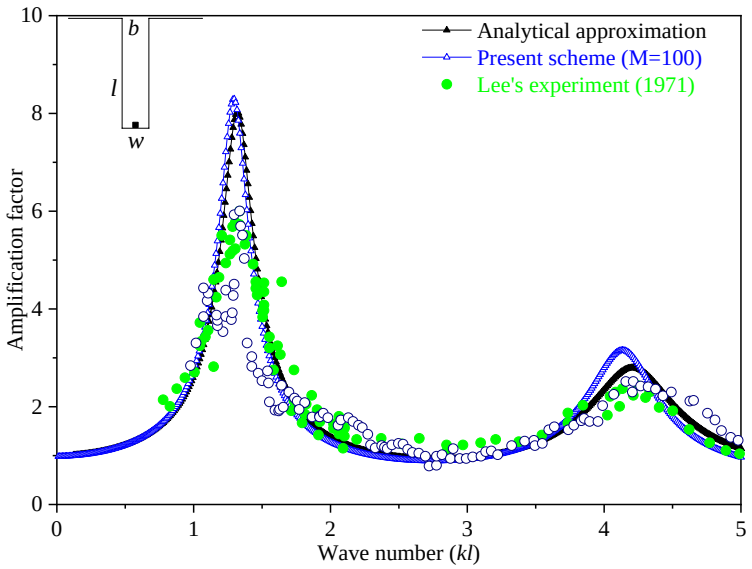

FIGURE 3. Validation of present model with Lee (1971)'s experiment data and analytical approximation.

SIMULATION RESULTS

Amplification Factor

Paradip Port ($20^o-15'-55.14"N$ & $20^o-14'-27.34"E$) is a deep water port situated in Jagatsinghpur district of Odisha, India. At present, it handles various Cargo like Thermal Coal, Coking Coal, Charge Chrome, Ferro Chrome, Crude oil, Iron Ore and many more. This port might plan to increase its cargo capacity from 118.5 million metric tons per annum (mmt) to 325 mmt to become India's biggest port. The simulation results and their better approximation with the previous studies enable us to execute our current numerical scheme on Paradip port for the evaluation of amplification factor. The amplification factor is demonstrated for irregular boundary discretization M=1215 corresponding to $\theta = \pi/2$ over Paradip port (see Fig. 5).

FIGURE 4. Bird view of the Paradip port, Odisha and two record stations are considered as R_1 and R_2 and red arrows show the incident waves propagating toward harbor's entrance.

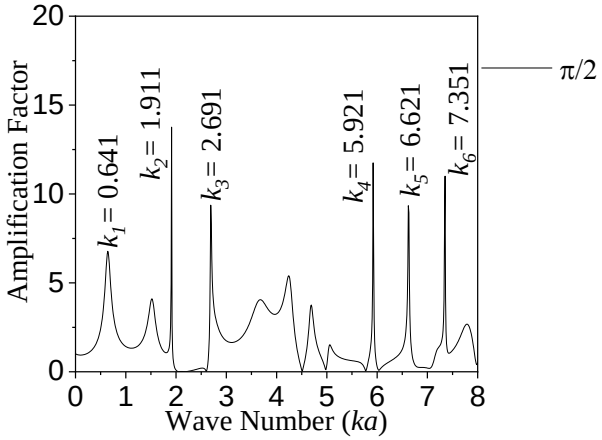

FIGURE 5. Amplification factor at Paradip port boundary with respect to the wave number (ka). The resonance frequencies are obtained at k_1, k_2, k_3, k_4, k_5 and k_6.

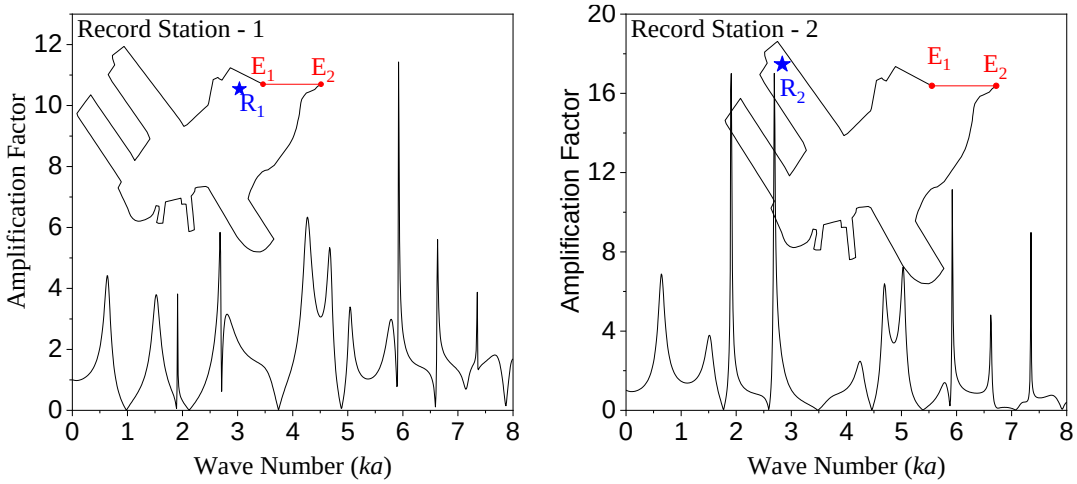

FIGURE 6. Amplification factor at Record station-1 and 2 inside the Paradip port for incident waves at angle $\theta = \pi / 2$

The frequencies (resonance modes) are calculated at Paradip port with frequency difference $\Delta k = 0.01$. The response of the amplification factor for incident waves is studied corresponding to waves propagating at $\theta = \pi / 2$. The higher amplification peaks are sharp and narrow whereas low amplification peaks are wider. A strong amplification for an incident wave directed at $\theta = \pi / 2$ is obtained for k_1 and k_2 resonance modes. We also analyze the amplification factor of two record stations R_1 and R_2 in Paradip port depending upon the loading and unloading of the moored ships as shown in Fig. 4. The record stations R_1 and R_2 are situated at the key port locations. It is observed that the record station R_2 has high amplification as compared to that of R_1 as shown in Fig. 6. Extreme resonance inside the port due to the matching of resonance frequency of incident waves with the natural port frequency could result in coastal hazards. To determine the safe location for the moored ships in Paradip port, it is imperative to evaluate the wave amplification precisely at the resonance modes. Incoming waves with distinct resonance modes and directions have variable impacts at the port. Thus, it has been observed that incident waves from east direction possess greater amplification than other directional waves.

Ocean Surface Wave Field

Direct incoming incident waves at key location of the port generate high resonance. The topographical features of Paradip port are considered corresponding to incident waves at $\theta = \pi / 2$ to deduce the wave field. Discretizing the boundary of the port as M=1215 segments with P=80 segments on the harbor entrance with two record stations R_1 and R_2, Fig. 7 represents the regularly distributed points by red dots. Ocean surface wave field is evaluated for two modes k_1 and k_2. The wave field response for k_1 and k_2 is shown in Fig. 7 with incident wave at $\theta = \pi / 2$ .Thus, the incident wave direction plays an crucial role inducing the wave amplification.

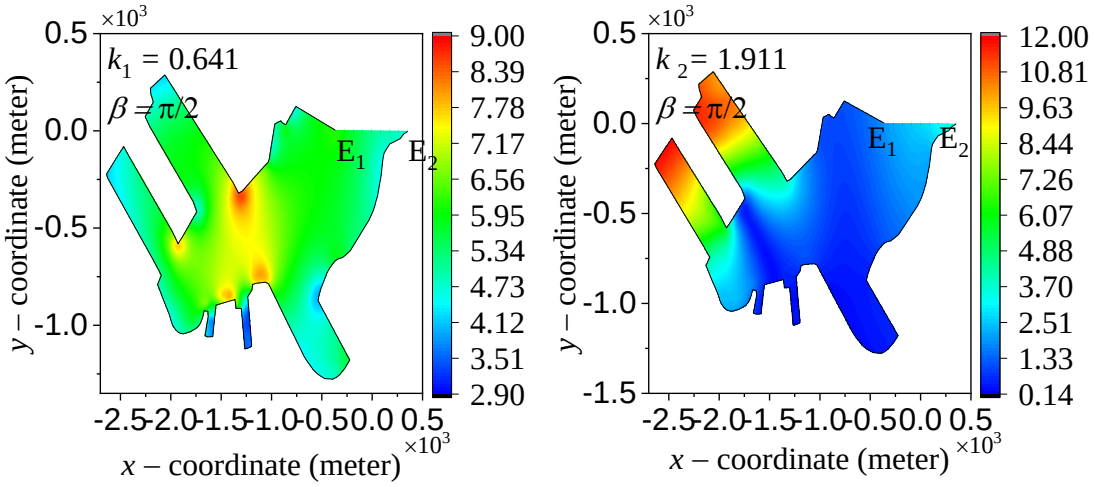

FIGURE 7. Ocean surface wave contours at resonance modes k_1 and k_2 for directional incident wave angle.

CONCLUSION

Paradip port, Odisha, India experiences wave induced oscillations of about 3-5m during the high amplitude incident waves. Under the resonance conditions, an efficient system is developed to study the port problem with refined corner points. The numerical model is validated with the Lee's experiment (1971) and the analytic approximations. It is concluded that the incident wave propagating at an angle $\theta = \pi / 2$ in the east direction have the highest amplification. Also, the incoming waves from Northeast direction produce less resonance in comparison to the incoming waves from east direction ($\theta = \pi / 2$). In order to prevent the damage of coastal structures, it is important to analyze the direction of incident waves and amplification factor to investigate safe locations at the Paradip port.

ACKNOWLEDGEMENT

This work is supported by the SERB-DST project no.: "ECR/2016/001680" and also supported by Department of Applied Sciences (Mathematics), National Institute of Technology, Delhi.

REFERENCES

1. G. Arfken, *Mathematical methods for physicists, Hankel function* (*3rd ed.*), (Academic press, London, 1985), pp. 101-1008.
2. G. Bellotti and L. Franco, Ocean Dyn. **61**, 2051-2059 (2011).
3. J.C.W. Berkhoff, "Computation of combined refraction-diffraction", In Proc. 13th Int. Conf. Coast. Eng. (ASCE, Canada, 1973), pp. 471-490.
4. L. Hwang and E.O. Tuck, J. Fluid Mech. **42**, 447 (1970).
5. A.T. Ippen and Y. Goda, Report No. **59**, Hydrodynamics Laboratory, MIT, (1963).

6. J.A. Zelt & F. Raichlen, J. Fluid Mech. **213**, 203-225 (1990).
7. L. Zhang & L. Billy, J. Coast. Res. **14**, 604-609 (1998).
8. A. Cerrato, J.A. Gonzalez & L.R. Tembleque. Eng. Anal. Bound. Elem. **62**, 22-34 (2016).
9. G. Y. Chen, C. C. Chien, C. H. Su, and H. M. Tseng, J. Oceanogr. **60**, 1035-1043 (2004).
10. T.A. Cruse, Comput. Methods Appl. Mech. Eng. **62**, 227-342 (1987).
11. J.J. Lee, J. Fluid Mech. **45**, 375-394 (1971).
12. H.S. Lee, Eng. Anal Bound. Elem. **28**, 1149-1155 (2004).
13. C. Lee, G. Kim and K.D. Suh, Coast. Eng. **53**, 311-318 (2006).
14. G. Dong, J. Gao, X. Ma, G. Wang & Y. Ma, Ocean Eng. **68**, 38-46 (2013).
15. M. Guerrini, G. Bellotti, Y. Fan, and L. Franco, Appl. Ocean Res. **48**, 322-330 (2014).
16. K. Hamanaka, Coast. Eng. **30**, 281-298 (1997).
17. P. Kumar, H. Zhang, and K.I. Kim, Pure Appl. Geophys. **171**, 1169-1185 (2014).
18. P. Kumar, H. Zhang, D.A. Yuen and K.I. Kim, Comput. Fluids **88**, 287-297 (2013).
19. P. Kumar and Gulshan, Pure Appl. Geophys. **174**, 4501 (2017).
20. M. Lopez, G. Iglesias, and N. Kobayashi, Appl. Ocean Res. **38**, 126 (2012).
21. P. Kumar and Gulshan, Ocean Eng. **164**, 13 (2018).
22. P. Kumar and Rupali, Ocean Eng. **165**, 386 (2018).